described above. This compares well with the particle size of cigarette smoke, which HINDS (1978) has reported to be less than 1·0 μm. The mean particle size was constant when concentrations of up to 1·80 mg ml^{-1} nicotine base in water were used, but as concentration increased, the variance increased to a maximum of 10 per cent.

The solution output was constant at 6·7 ml min^{-1} over a period of 2 h. The concentration of nicotine in the collected aerosol was 0·45 mg ml^{-1} (nicotine expressed as nicotine base), indicating no change from the original solution. This was verified by collecting and analysing the solution by gas chromatography (JACOB *et al.*, 1981).

When a concentration of nicotine in water of 0·45 mg ml^{-1} is used, the generator delivers 100 μg of nicotine every 2 s, allowing the inhalation of 100 μg of nicotine with each puff of aerosol. When 15 healthy male subjects were given the nicotine aerosol to inhale, the peak nicotine concentration in blood was 46 ± 7 nmoles l^{-1} (mean $\pm$ SE). The peak blood levels detected varied from 25 to 117 nmoles l^{-1}. This compares well with the blood levels achieved after smoking a single cigarette. Values reported in the literature range from 5 to 30 ng ml^{-1} or approximately 30 to 185 nmoles l^{-1} (ARMITAGE *et al.*, 1975; HERNING *et al.*, 1983; ISAAC and RAND, 1972).

4 Conclusions

The nicotine aerosol generated using this system is suitable for use in studies of inhaled nicotine. The small particle size, low nicotine concentration, low flow rate and low pH make the aerosol easy to inhale. By adjusting the concentration of nicotine in the solution, the dose administered can be varied. The advantages of this system over other atomisers are that a submicrometre particle size is easily attained, the system does not become clogged, the concentration of nicotine in the aerosol has been measured to be constant over a 2 h period, and the mass output is high. The nicotine aerosol is easily inhaled to produce substantial concentrations of nicotine in blood.

Acknowledgment—This study was supported by grants from the Ontario Ministry of Health and from the Natural Sciences & Engineering Research Council (Canada). The results and conclusions presented here are those of the authors, and no official endorsement by the Ontario Ministry of Health or Addiction Research Foundation is intended or should be inferred.

References

ARMITAGE, A. K. and TURNER, D. M. (1970) Absorption of nicotine in cigarette and cigar smoke through the oral mucosa. *Nature*, **226**, 1231–1232.

ARMITAGE, A. K., DOLLERY, C. T., GEORGE, C. F., HOUSEMAN, T. H., LEWIS, P. J. and TURNER, D. M. (1975) Absorption and metabolism of nicotine from cigarettes. *Br. Med. J.*, **4**, 313–316.

BENOWITZ, N. L., JACOB, P., JONES, R. T. and ROSENBERG, J. (1982) Interindividual variability in the metabolism and cardiovascular effects of nicotine in man. *J. Pharmacol. Exp. Ther.*, **221**, 368–372.

DOLOVICH, M., RYAN, G. and NEWHOUSE, M. T. (1981) Aerosol penetration into the lung. *Chest* **800**, 834.

HERNING, R. I., JONES, R. T., BENOWITZ, N. L. and MINES, A. H. (1983) How a cigarette is smoked determines nicotine blood levels. *Clin. Pharmacol. Ther.*, **33**, 84–90.

HEYDER, J. (1982) Alveolar deposition of inhaled particles in humans. *Am. Ind. Hyg. Assoc. J.*, **43**, 864–866.

HINDS, W. C. (1978) Size characteristics of cigarette smoke. *Ibid.*, **39**, 48–54.

ISAAC, P. F. and RAND, M. J. (1972) Cigarette smoking and plasma levels of nicotine. *Nature*, **236**, 308–310.

JACOB, P., WILSON, M. and BENOWITZ, N. L. (1981) Improved gas chromatographic method for the determination of nicotine and cotinine in biologic fluids. *J. Chromatography*, **222**, 61–70.

KARASEK, F. W. (1978) Cascade particle analyzer. *Ind. Res. Dev.*, Oct, 154–159.

RUSSELL, M. A. H., FEYERABEND, C. and COLE, P. V. (1976) Plasma nicotine levels after cigarette smoking and chewing nicotine gum. *Br. Med. J.*, **1**, 1043–1046.

RUSSELL, M. A. H., JARVIS, M. J., FEYERABEND, C. and FERNO, O. (1983) Nasal nicotine solution: a potential aid to giving up smoking? *Ibid.* **286**, 683–684.

Technical note

Programmable dynamic muscle load for animal experiments

P. H. Veltink J. E. van Dijk J. A. van Alsté

Biomedical Engineering Group, Department of Electrical Engineering, Twente University, PO Box 217, 7500 AE Enschede, The Netherlands

Keywords—*Control of muscle contraction, Dynamic muscle load, Programmable mechanical impedance*

Med. & Biol. Eng. & Comput., 1988, **26**, 234–236

1 Introduction

IN FUNCTIONAL ELECTRICAL stimulation (FES) contraction of paralysed muscles is controlled by means of artificial electrical nerve stimulation. For animal research on control of muscle contraction with FES it is desirable to have the muscle connected to a defined mechanical load (VELTINK *et al.*, 1986). Physiological experiments on skeletal muscle contraction for FES mostly concern isometric contractions (WILHERE *et al.*, 1985; BERNOTAS *et al.*, 1986). Experiments with a defined dynamic mechanical load connected to the muscle are rare (PETROFSKY and PHILLIPS, 1979; ALLIN and INBAR, 1986*a*;*b*).

First received 16th February and in final form 22nd September 1987

We have made a programmable dynamic load system for experiments on contraction control for hind limb muscles of small animals.

2 Principle of operation

A mechanical muscle load can be defined as a dynamic relationship between force F and position x, where x is the position of the end of the muscle tendon that is connected to the mechanical load (Fig. 1). In this note a second-order load model will be used as an example:

$$F = M\ddot{x} + D\dot{x} + Cx + F_a \quad (1)$$

Model parameters are M (mass), D (damping constant), C (compliance) and F_a (antagonistic muscle force or offset force).

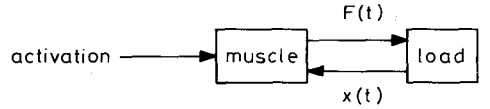

Fig. 1 *Schematic drawing of a mechanical load connected to a muscle. The force signal F(t) is input for the load and the position signal x(t) is output*

The force F can be considered as the input signal and the position x as the output signal. In this way eqn. 1 can be calculated in a simulation scheme with two subsequent integration operations, as shown in Fig. 2. This scheme is easier to realise than a scheme with two subsequent differentiation operations, as would be obtained when position was the chosen input signal.

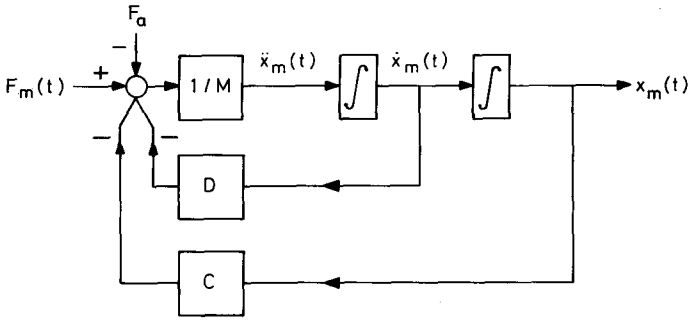

Fig. 2 *Block diagram of the second-order simulation model:*

$$F_m = M\ddot{x}_m + D\dot{x}_m + Cx_m + F_a$$

M	*mass*
D	*damping constant*
C	*compliance*
$F_m(t)$	*measured muscle force*
$x_m(t)$	*position computed by the model*
F_a	*offset force or antagonistic muscle force*

The real-time calculation of the load model has been realised by a microprocessor system. The input signal of the processor is the force signal that is obtained from a force transducer. The output of the load simulation is the position signal, which is the input for the position actuator, a servo-controlled linear motor system. The model in the load simulator is loaded from an external computer (Fig. 3).

3 Realisation

The force transducer consists of a bridge configuration of four strain gauges on a thin steel bar connected to a bridge amplifier. The force transducer is connected to a muscle tendon and is situated on the moving part of the position actuator.

The position actuator was realised by a servo-controlled linear motor system. The linear motor originated from the read/write head positioning of a computer disk drive and

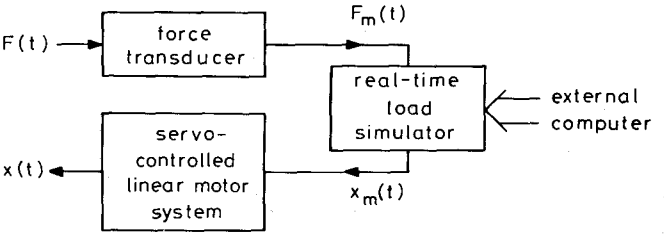

Fig. 3 *Block diagram of a real-time mechanical load simulator*

$F(t)$	*muscle force*
$f_m(t)$	*measured muscle force*
$x_m(t)$	*position computed by the model*
$x(t)$	*imposed position*

was characterised by a current-to-force transfer of about 4 N A^{-1}. A servo-control system was constructed, having an outer position feedback loop, containing a controller of the proportional-integration type and an inner tacho feedback loop. The position feedback signal is measured with a digital optical position transducer with a resolution of about 30 μm. An inductive velocity transducer is used in the tacho loop.

The load processor consists of a 6502 microprocessor system and an AM9511 floating-point mathematical co-processor. The load processor internally uses a 2 byte floating-point representation, because of the large differences in values to be used. The load simulator is controlled by an external computer, an LSI 11/23. Load algorithm and load parameters can be generated on this computer and downloaded to the load processor. This provides the possibility to realise different loads, using different simulation algorithms.

4 Results

Responses of the servo-controlled linear motor system to steps of 1·5 mm in the position signal have a risetime of about 5 ms and a settling time of about 15 ms.

The computing frequency f_c for the load model was taken as the same as the sample frequency of the force signal f_s. With our load simulator the second-order load model (eqn. 1) can be computed up to 385 times per second ($f_{c,max}$ = 385 Hz). The bandwidth of a realistic load model f_{BL}, and hence the bandwidth of the length signal, is less than 50 Hz. The bandwidth of the force signal is about 150 Hz. The bandwidth of the force signal after presampling filtering f_{BF} can be taken smaller.

More complex load models, requiring a longer computation time, can be simulated. A longer computation time results in a lower maximum computing frequency $f_{c,max}$. The minimum computing frequency $f_{c,min}$ determines the maximum model computation time allowed. Aliasing in the force signal in the frequency range above the passband of the load model is stopped, and consequently does not effect the position signal, so a sufficient criterion for avoiding aliasing errors in the computed position signal is

$$f_c > f_{BL} + f_{BF} \quad (2)$$

This yields a minimum computing frequency $f_{c,min}$ of 200 Hz without, and an even lower frequency with presampling filtering of the force signal.

The time discrete calculation of the load model yields a distortion of the transfer function of the simulated time continuous model. We measured an error of 5 per cent in the modulus and 8° in the argument of the transfer function at 10 Hz for a critically damped second-order model with a resonance frequency for zero damping of 7 Hz and a calculation frequency of 200 Hz. At a calculation frequency of 350 Hz these errors were 0·6 per cent and 0°. The distortion of the transfer function is caused by the time-discrete

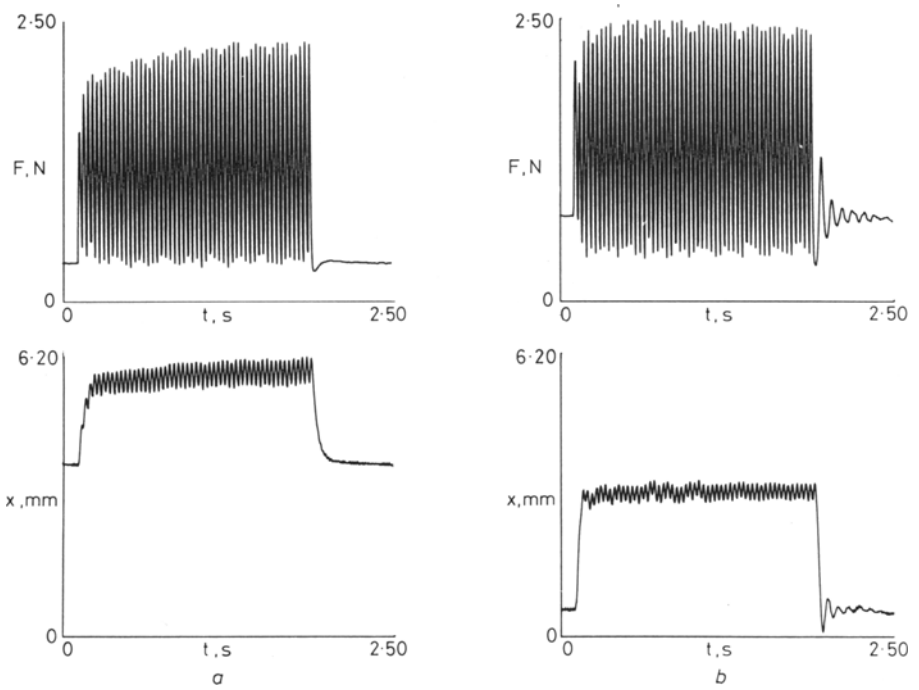

Fig. 4 *Force and length signals for two sets of parameters of the second-order load model (eqn. 1) during 2 s supramaximal stimulation at 30 Hz. Position x increases for shortening muscle. The parameters are (a) $M = 0{\cdot}12\,kg$, $D = 32{\cdot}6\,N\,s\,m^{-1}$, $C = 463\,N\,m^{-1}$, $F_a = -1{\cdot}40\,N$; (b) $M = 0{\cdot}41\,kg$, $D = 13{\cdot}0\,N\,s\,m^{-1}$, $C = 260\,N\,m^{-1}$, $F_a = 0{\cdot}60\,N$*

integration algorithm, the calculation time of the load model and the reconstruction filter. The time-discrete integration algorithm is an approximation of time-continuous integration. We used the Euler integration algorithm. Besides by using a higher calculation frequency f_c, these errors can be reduced by a more accurate integration algorithm. However, this is at the cost of more computation time. The time necessary for calculating a sample of the length signal according to the load model introduces a time delay. This results in an extra phase shift proportional to frequency in the transfer function. The time delay can be decreased by using a faster processor. Errors in analogue signal reconstruction can be reduced by a higher calculation frequency or a more accurate reconstruction filter. We used a zero-order reconstruction filter, a hold circuit.

Fig. 4 shows some experimental results of stimulating a mechanically loaded muscle. The tibialis anterior muscle of a hindlimb of a rat was stimulated supramaximally via the peroneus communis nerve at 30 Hz for 2 s. Further details on the experimental methods used can be found in VELTINK *et al.* (1986). Muscle force and length signals for two sets of parameters of a second-order load model (eqn. 1) are shown in Fig. 4. The resonance frequency of the load for zero damping was 9·9 Hz in Fig. 4*a* and 4·0 Hz in Fig. 4*b*. The rest length, when the muscle is not contracting, differs for both figures. The load model of Fig. 4*a* is damped supercritically, whereas the load of Fig. 4*b* is subcritically damped. As can be seen in the force signals, the load characteristics not only determine the length signal, but also influence the force signal, because of the length and velocity dependency of the muscle dynamics.

5 Conclusion

We constructed a mechanical load system for physiological experiments, for instance on contraction control of artificially stimulated muscle. The load characteristics, determined by the load algorithm and the load parameters, can be changed flexibly. The load system provides the opportunity to investigate strategies for the control of muscle contraction (e.g. muscle length control) under the conditions of an artificially stimulated muscle and a realistic mechanical load.

Acknowledgments—We would like to thank E. M. J. Wilms, B. J. Oderkerk and R. Putman for their help in making the load stimulation system and J. Put for assistance in the animal experiments.

References

ALLIN, J. and INBAR, G. F. (1986*a*) FNS parameter selection and upper limb characterization. *IEEE Trans.*, **BME-33,** 809–817

ALLIN, J. and INBAR, G. F. (1986*b*) FNS control schemes for the upper limb. *Ibid.*, **BME-33,** 818–828

BERNOTAS, L. A., CRAGO, P. E. and CHIZECK, H. J. (1986) A discrete-time model of electrically stimulated muscle. *Ibid.*, **BME-33,** 829–838.

OPPENHEIMER, A. V. and SCHAFER, R. W. (1975) *Digital signal processing.* Prentice-Hall, Englewood Cliffs, New Jersey.

PETROFSKY, J. S. and PHILLIPS, C. A. (1979) Constant-velocity contractions in skeletal muscle by sequential stimulation of muscle efferents. *Med. & Biol. Eng. & Comput.*, **17,** 583–592.

VELTINK, P. H., VAN DIJK, J. E. and VAN ALSTÉ, J. A. (1986) Contraction control of a mechanically loaded muscle during artificial nerve stimulation. Proc. 2nd Vienna Int. Workshop on Functional Electrostimulation, 231–234.

WILHERE, G. F., CRAGO, P. E. and CHIZECK, H. J. (1985) Design and evaluation of a digital closed-loop controller for the regulation of muscle force by recruitment modulation. *IEEE Trans.*, **BME-32,** 668–676.